









PAPER

View Article Online
View Journal | View Issue

Cite this: *Nanoscale Adv.*, 2021, 3, 675

Dynamic degradation of metallic nanowire networks under electrical stress: a comparison between experiments and simulations

Nicolas Charvin, ^a Joao Resende, ^b Dorina T. Papanastasiou, ^b David Muñoz-Rojas, ^b Carmen Jiménez, ^b Ali Nourdine, ^a Daniel Bellet ^b and Lionel Flandin ^{*a}

Metallic nanowire networks represent a promising solution for a new generation of transparent and flexible devices, including touch screens, solar cells and transparent heaters. They, however, lack stability under thermal and electrical stresses, often leading to the degradation of nanowires, which results in the loss of electrical percolation paths. We propose a comprehensive description of the degradation mechanism in a metallic nanowire network subjected to electrical stress. The nanowire network degradation is ascribed, at a very local scale, to the hot-spot formation and the subsequent propagation of a spatially correlated disruptive crack. We compare the behaviour of actual networks under electrical and thermal stresses to dynamic simulations of randomly deposited sticks on a 2D surface, and a thermal phenomenon simulated in a metal thin film. On one hand, such comparison allows us to deduce an average junction resistance between nanowires. On the other hand, we observed that initial flaws in a discrete network result in a local current density increase in the surrounding area, further leading to an amplified Joule effect. This phenomenon promotes the spatial correlation in the damage of the percolating network. Such non-reversible failure of the transparent electrode is in good agreement with experimental observations.

Received 26th October 2020
Accepted 30th November 2020

DOI: 10.1039/d0na00895h

rsc.li/nanoscale-advances

Introduction

The growing interest in flexible, efficient and low cost transparent electrodes has prompted the development of alternative solutions^{1,2} to transparent conductive oxides.³ In this matter, metallic nanowire networks exhibit outstanding properties, with sheet resistance values below $10 \Omega \text{ sq}^{-1}$, optical transparency of 90% and mechanical stability under repeated bending tests when deposited on flexible substrates.^{4,5} In particular, silver nanowire (AgNW) networks have been largely studied and already used as efficient transparent electrodes for solar cells,⁶ organic light emitting diodes,⁷ sensors,⁸ or as the main active material for transparent heaters (THs).⁹ AgNW networks possess several promising assets: the requirement of a small quantity of silver ($\sim 0.1 \text{ g m}^{-2}$), compatibility with low-cost solution-based deposition methods and excellent electrical and optical properties which can be combined with a unique flexibility.

However, AgNW networks tend to degrade under electrical and thermal stresses, especially for the very demanding transparent heater applications but also for solar applications.¹⁰ The

observed degradation, at the macroscopic scale, is described as a failure of the networks.^{11–14} For thermal instability, the degradation of the nanowires can be described as a fragmentation (or spheroidization) of the wires, described by the Plateau-Rayleigh instability: the associated driving force is the surface energy minimization of nanowires, causing the transformation into more spherical nanoparticles.^{10,13} Electromigration, which also has an effect on nanowire network transformation, can be defined as material migration caused by an electrical field.¹⁵ This phenomenon has many consequences in electrical interconnects in integrated circuits¹⁵ and has also been reported for AgNW networks.^{16,17} Nevertheless, electromigration will not be thoroughly considered in the present paper. Conversely to thermally induced instability which affects uniformly the whole specimen; during electrical breakdown, Sanniccolo *et al.* showed that damage to the AgNW network is localized in a region called “network crack”, which spreads in a direction roughly parallel to opposite electrodes until reaching either sample edges.¹⁴ The sample has eventually lost its main conducting property. The crack propagation is time dependent and its growth can be directly tracked with an infrared (IR) camera.¹⁴

Successful simulations of metallic nanowire networks have been described with a random arrangement of linear sticks on a 2D surface.^{18–24} These models predict different macroscopic properties fairly well, such as optical transparency, percolation

^aUniv. Grenoble Alpes, Univ. Savoie Mont Blanc, CNRS, Grenoble INP, LEPMI, 38000 Grenoble, France. E-mail: lionel.flandin@univ-smb.fr

^bUniv. Grenoble Alpes, CNRS, Grenoble INP, LMGP, 38000 Grenoble, France


threshold and macroscopic resistance. Very few parameters are necessary to describe the challenging law of the percolation theory:¹³ the linear resistance of a single nanowire, and an estimation of the junction resistance between nanowires in contact. This kind of model has, up to now, been developed with static networks presenting different densities, essentially to compare with the well-known power law equation of the percolation theory.

The next step requires further understanding of the failure mechanisms and the potential consequences encountered during usage conditions for the different applications mentioned above. This requires the development of computation methods, and their calibration and thorough comparison with experimental results. The present work consists of enhancing models towards a time dependent simulation, including structural changes within the resistive network to mimic its progressive degradation under electrical stress. The proposed dynamic approach is based on the evaluation of the current distribution on a simulated network. A stepwise change in the microstructure of the network is then applied to account for the degradation of the most stressed links, at the AgNW scale. This allows a dynamic simulation of the alterations of the stressed network. The obtained local hot-spot formation and crack propagation, in agreement with experimental results, do induce a direct adjustment of the macroscopic resistance. Additionally, we simulated the thermal and electrical properties of a macroscopic system with a well-defined initial defect, using a thin metallic film as a model.

Experimental procedure and simulation description

Silver nanowire network deposition

AgNWs with an aspect ratio close to 100 (average diameter of 70 ± 10 nm and average length of 8 ± 3 μm) were kindly provided from the research team of Jean-Pierre Simonato from CEA-LITEN in Grenoble, France, being produced as detailed in Mayousse *et al.*²⁵ Squared borosilicate Corning glass (1737) was used as a substrate, with a size of 25×25 mm². Before AgNW deposition, the substrates were sonicated during 15 minutes in isopropanol, rinsed with distilled water, and finally dried with N₂ gas. The deposition of the AgNW networks was conducted via spray-deposition using a home-made spray set-up composed of an airbrush (Harder & Steenbeck), a robotic arm and a heating plate. A suspension of AgNWs in methanol with a concentration of 0.1 g L^{-1} was used, and N₂ was used as a spraying gas with a pressure of 1.4 bar. The substrates were heated at 110 °C to easily evaporate the solvent, and the density of the network was attained by controlling the number of spray cycles. 2 mm wide silver-paste electrodes were added on two opposite sides of the samples (by convention these contacts are vertical in all figures of the present article). Fig. 1a, b and c exhibit a picture, optical microscope image and SEM image, respectively, of a typical randomly deposited AgNW network, with a corresponding areal mass density (*amd*) of 93 mg m^{-2} .

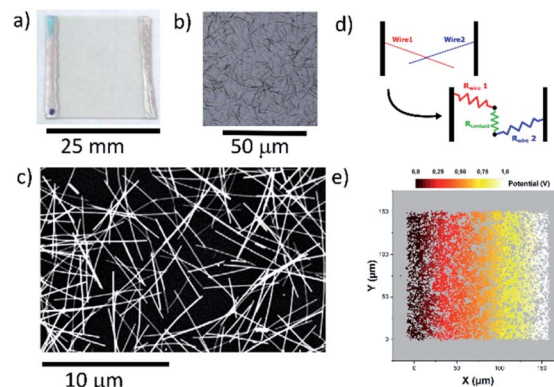


Fig. 1 Deposited AgNW networks on glass and scheme of the computational simulation. (a) Picture of a 25×25 mm² AgNW network on glass with electrodes on opposite edges. (b) Optical microscope image of the randomly deposited AgNW network. (c) SEM image of the AgNW network with nanowires of an average length of 8 μm and a diameter of 70 nm with a corresponding *amd* of 93 mg m^{-2} . (d) Scheme of two intersecting nanowires, and how R_{wire} and R_{contact} are considered in the simulation model. (e) Representation of a AgNW network (150×150 μm^2) with a colour map representing the electrical potential under an applied voltage bias of 1 V between opposite vertical electrodes.

Characterization techniques

The AgNW morphology was analysed by using an Optical Microscope (Leica DM LM) and with two Field Emission Gun-Scanning Electron Microscopes (FEG-SEM Environmental FEI QUANTA 250 and Zeiss GeminiSEM 300). The *amd* of the network was measured from 10 SEM images, using ImageJ software and the Skeletonize plugin.

All electrical measurements were performed using a Keithley 2400 source-measure-unit (SMU), in a 4-wire configuration. A current sweep from 0.1 to 10 mA was initially performed to extract the sheet resistance of the sample, R_s , from a linear fit on the $V(I)$ curve. All samples exhibited a perfectly ohmic behaviour under any circumstances. Then a degrading voltage ramp was applied at 1 V min^{-1} from 3 V up to the beginning of the breakdown. The SMU was then switched to constant-current mode, to perform continuous resistance measurements. For measuring electrical resistance the source level was set at 1 μA , to minimize the electrical stress on the sample resulting from the current flow itself. Meanwhile, an *in situ* IR imaging of the sample was performed, to record the temperature distribution on the sample area (from which the maximum temperature, T_{max} , can be extracted), using a FLIR A320G IR camera placed above the setup. During all the electrical tests, the samples were held hanging in mid-air. The resulting heat-transfer processes could explain the wave-like temperature distribution along the X-direction, when one could expect a homogeneous distribution all over the sample.

Computational models

Electrical model. The model was developed with a home-made Python code. As mentioned above, a metallic discontinuous nanowire network may be simulated with a random



arrangement of 2D segments on a rectangular area ($L_{sx} \times L_{sy}$).^{23,26} We used the same approach to generate the AgNW network model. Each stick was further discretized at the intersection points with others. Two kinds of resistances were then defined depending on their locations: each sub-segment was transformed into a wire resistor (R_{wire}), whereas each intersection was represented as a contact resistor ($R_{contact}$), as schematically represented in Fig. 1d. The sample thereby becomes a purely resistive network, represented by using a graph.²⁷ Each edge of this graph is a resistor representing either part of a AgNW or a contact between two of them. Lagrange *et al.*¹² showed that the AgNW length and diameter may be reduced to an intrinsic linear resistance, R_{lin} , based on the intrinsic resistivity of AgNW.²⁸ The value of each wire resistance is proportional to the length of the corresponding sub-segment. The contact resistance R_c between two intersecting segments is a key parameter in any nanowire network model, and it has been extensively studied.^{24,29} The R_c value could either be determined for individual junctions by direct measurements,³⁰ or assumed as an average R_c value by adjusting the simulated sheet resistance of the sample, R_s , in order to mimic the real characteristics of similar experimental networks, using R_c as a fitting parameter.³¹ The latter approach has been used in this paper. Once the model is completed, the adjacency of the network, (x , y) coordinates of all nodes and values of all resistors are self-contained in the graph structure, as well as the voltage source level between electrodes. The electrical potential value can then be calculated on every node of the graph using Kirchhoff's Current Law (KCL). This then results in a unique and unambiguous electrical potential map over the whole sample as represented in Fig. 1e, and a corresponding sheet resistance of the sample, R_s . The correct scaling of the model has been verified, by changing the sample dimensions. This method enables a straightforward comparison between modelled and experimental samples. The main requirement is the good correspondence between the geometrical features, namely the nanowire characteristics (diameter and length), the size of the sample ($L_{sx} \times L_{sy}$), and the network density. The latter can be defined through different approaches. Within the AgNW community the network density, n , is often defined as the number of AgNWs per unit area, $n = N_w/(L_{sx} \times L_{sy})$, where N_w is the total number of AgNWs; however such density does not account for the AgNW size. Another approach considers the *amd*, which is simply the product of n by the average mass of one AgNW. In this work, we follow the approach reported by Forró *et al.*,²³ in which the normalized density of the sticks D is used, where $D = N_w \times L_w^2/(L_{sx} \times L_{sy})$, with L_w the average AgNW length. It is worth noting that these three network densities are proportional to each other, and therefore any of them could be used without modifying the physical meaning of the model.

The Joule effect states that any electrical current flowing through a conductor induces heating. It has been shown that it is still valid for nanowires³² and it is currently used in transparent heaters based on metallic nanowires.⁹ We consider the degradation of a single AgNW at a microscopic level to be directly linked to the temperature of that particular wire. This temperature is directly dependent on the energy dissipated in

the wire. An iterative damage phenomenon was thus simulated at a very individual and local scale by progressively and irreversibly modifying the nanowire network model, depending on the thermal destruction of single wires. The model only alters the percolation cluster, thanks to the underlying graph structure. Under a given voltage bias, the electrical current density j is determined in every resistor of the constructed graph (either R_{wire} or $R_{contact}$ type). At each iteration step, the resistor with the highest j , among all resistors whose j is larger than a defined threshold value $j_{failure}$, is selected. The corresponding resistor is then considered to be broken and removed from the graph. This process is repeated, until the network loses its percolating nature between the two opposite electrodes. The experimental critical current density $j_{failure}$ can be derived from the observed voltage bias $V_{failure}$ at which failure occurs on a real sample.¹² If the voltage bias is scaled according to the ratio ($L_{sx,simul}/L_{sx,exp}$), $j_{failure}$ can be used as a realistic threshold in the simulation.

Thermal model. In addition to the 2D stick percolation methods, COMSOL Multiphysics® (based on finite element analysis or FEA) was used to simulate macroscopically the electrical performance of AgNW networks as well as the locally induced increase of temperature. A model close to a real-size AgNW network sample was created. The main objective was to compare the effect of the macroscopic temperature from a numerical and an experimental standpoint. The FEA computation limits imposed a simplified model, therefore a thin Ag layer was utilized in place of the discrete AgNW network. The thickness of the homogenized layer (for instance 10 nm) was chosen to use a similar amount of metal than the discrete one (for instance an *amd* of 105 mg m⁻²). With this method, the size of the simulated specimens is the same as that of the experimentally fabricated ones (25 × 25 mm²), with the same Corning glass substrate (25 × 25 × 1.1 mm³). The modules “Electric Currents, Shell” and “Heat transfer in solids” of the AC/DC COMSOL model were used for the computations. The electrical and heat properties and thermal coefficients of thin Ag and Corning glass were applied.

Results and discussion

The random deposition of AgNWs on a glass substrate results in transparent samples, as shown in Fig. 1a. Optical microscope images and SEM micrographs, represented respectively in Fig. 1b and c, show a network composed of AgNWs with an average nanowire length of 8 μm and a diameter of 70 nm with a corresponding *amd* of 93 mg m⁻², and an initial macroscopic resistance of 8.9 Ω, similar to previous studies.^{30,31}

In order to compare with the deposited sample, the scheme of the numerically simulated nanowires is represented in Fig. 1d. Two different segments are represented with the additional contact resistance in-between. The density of the simulated network was that of the equivalent experimental sample ($D_{exp} = 18.5 \pm 0.9$ in this case). The intrinsic linear AgNW resistance value was determined to be $R_{lin} = 5.1 \Omega \mu m^{-1}$. The contact resistance, also called junction resistance, was estimated by performing many simulations with the proposed model. Assuming the other parameters (sample dimensions,



network density and intrinsic linear resistance of nanowires) are well-determined, simulations were run for varying R_c values. As shown in Fig. 2, R_s can then be represented as a linear function of R_c . Knowing the experimental sample sheet resistance, and expecting the simulated one to be the same, one can directly estimate $R_c = 14 \pm 2 \Omega$. This value is in accordance with the ones in the literature for optimized nanowire junctions.³¹ The main source of uncertainty in the determination of R_c is the extraction of D_{exp} from SEM images that should closely represent the macroscopic density of the considered sample. As summarized by Bellew *et al.*,³¹ contact resistance is spread over a continuous distribution, ranging from a few ohms to several kilo-ohms. Nevertheless, as stated above, R_c will be considered here as a constant average value for the sake of simplicity. Fig. 1e shows the potential distribution for a nanowire network in a square specimen ($150 \times 150 \mu\text{m}^2$) subjected to 1 V. The equipotential lines are reasonably straight and parallel to the opposite electrodes. The simulated map therefore suggests a homogeneous sample.¹⁴ This is confirmed by a linear change of the voltage from the left electrode to the right one and its sole dependence on the horizontal position. The underlying discrete nature of the network appears therefore to be screened at this macroscopic scale; with such a network density, the network essentially behaves like a continuous layer.

The deposited network was subjected to a continuous voltage ramp, with bias values large enough to degrade the network, as shown in Fig. 3a. As the voltage increases, so does the temperature, due to the Joule effect; the metallic nature of the conducting element leads to a slight increase of the resistance as temperature increases. The induced heating is confirmed by the temperature measured by using an IR camera; the maximum observed temperature, T_{max} , is also reported in

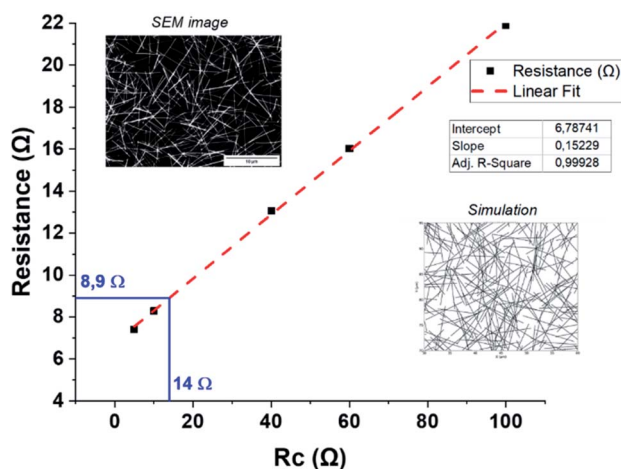


Fig. 2 Determination of the average contact resistance between AgNWs: the simulated network sheet resistance is plotted *versus* the contact resistance (R_c) between two AgNWs. The computed R_s value is finally adjusted to the experimental one, leading to the correct estimated R_c value. SEM pictures of AgNW networks are used to extract the network density. For each arbitrary R_c value, 50 simulations were performed in order to average the randomness of the simulated networks.

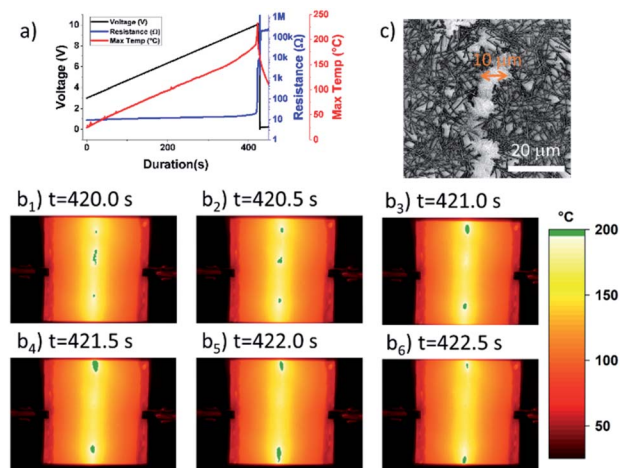


Fig. 3 Experimental observation of the degradation of a spray deposited AgNW network. (a) Time evolution of resistance and maximum temperature on a AgNW network sample with an initial resistance of 8.9Ω when applying a voltage ramp of 1 V min^{-1} , starting from 3 V, until voltage breakdown was observed around 10 V. (b₁–b₆) Infrared images corresponding to the crack formation during the voltage ramp at different times between 420 and 422.5 s. Green areas represent the hottest regions, above 195°C . A visible propagation of the hot-spot from the centre of the specimen to the edges, following a parallel line to the vertically aligned electrodes, is observed. (c) SEM image of the AgNW network degradation or “crack” visible due to the differences in the charging effect on the secondary electron detector. The width of the crack is about $10 \mu\text{m}$.

Fig. 3a. When the voltage bias reaches about 10 V, around 420 seconds after the beginning of the experiment, a significant and sharp increase in the resistance values is evidenced. Indeed, in less than 10 seconds, a sharp increase of five orders of magnitude is observed (from 10Ω to $\text{M}\Omega$). This is simultaneously accompanied by a sharp increase of T_{max} , as shown in Fig. 3a. The series of IR images in Fig. 3b reveals that the location of the degradation also moved quickly throughout the entire sample. The green areas correspond to isothermal zones, *i.e.* where the temperature exceeds a specified threshold, here 195°C . According to the series of images, the hotspots gradually shift from the centre of the specimen to the top and bottom edges. The resulting path follows a somewhat linear course parallel to the opposite electrodes. This extensive propagation is consistent with the electrical resistance increase, until the moment where the network is largely damaged and the electrical percolation is not spanning anymore from one electrode to the other. However, as previously described,^{14,17} one might observe that R_s returns to the $1 \text{ k}\Omega$ range after some time at rest. The critical current density j_{failure} was determined to be $1.63 \times 10^{10} \text{ A m}^{-2}$. The latter is in good agreement with the discussion reported in Lagrange *et al.*¹² SEM images reveal a domain with degraded nanowires, where the network had been wiped out, as shown in Fig. 3c. These bands with a width of several μm , result from the local degradation of AgNWs and are at the origin of the sharp increase of the measured electrical resistance.

In order to establish a realistic simulation of this network evolution, a static 2D stick model was utilized to mimic the

undamaged state. A $200 \times 253 \mu\text{m}^2$ numerical sample was created for this purpose, with the same L_{sx}/L_{sy} ratio as the experimental substrate shown in Fig. 1a, and subjected to a 0.1 V voltage bias. The dynamic process described above was then applied to alter the simulated structure. The most stressed resistors were not scattered evenly across the sample. On the contrary, we observe a very strong geometric correlation within damaged resistors as the simulation progresses. In other words, the local breakdown of a resistor stresses the surrounding ones and makes them more likely to rupture during the following steps. This results in a well-defined and topologically controlled propagation process along a rather vertical crack (parallel to the electrodes), analogous to a mechanical crack. From the macroscopic standpoint, this induces the regular increase of the overall resistance of the system that was observed at each degradation step, as depicted in Fig. 4a. An example of the electrical current map is displayed in Fig. 4b after 75 steps corresponding to a macroscopic resistance of 16Ω . The image shows a crack that appeared and further expanded to the middle of the specimen. The effect of the crack formation on the voltage map is represented with a series of images in Fig. 4c. The tip of the crack may actually be identified on the map (Fig. 4b) as the location where the current exhibits its highest value. The crack may be initiated anywhere within the sample. In the present case it was in the centre: this initial position is purely guided by the random generation of the network and should not be directly interpreted. In contrast, the crack propagation across the specimen occurs continuously. The strong dependence between the successive degraded links is the direct consequence of the positive feedback loop between the link degradation and the increase of current in the surrounding nanowires.

In order to better understand the phenomenon controlling the crack propagation, simulated networks were prepared with

a well-defined notch. This flaw was first utilized to initiate the cracks on a known position, as shown in Fig. 5a. The notched specimens were modelled with the random stick simulation to determine the voltage and current maps, as described above. In addition, the surface current density and temperature of a homogeneous silver film with the same geometry were calculated using COMSOL Multiphysics software. In this simulation, the silver material was removed on a strip of $10 \mu\text{m}$ width. A 1 V voltage bias was then applied between the two opposite electrodes. As expected, the surface current density indicates a rather homogeneous distribution, except within the area that contains the notch, as clearly shown in Fig. 5b. In this case, the COMSOL simulation results in a 10 times increase of the current density at the tip of the defect, as compared to the homogeneous specimen case. A large tip-effect was already obtained, even for rather short notch of only $20 \mu\text{m}$ in length. This intense current density value results in a highly localized temperature increase, due to Joule heating. A steady-state temperature analysis is shown in Fig. 5c, with the sample still under a 1 V bias. This is the origin of the hotspot creation in an experimental AgNW network, as the temperature is higher in this region, causing a nanowire spheroidization and loss of electric contact.

Therefore, considering the destruction of the network as a coupling electrical/thermal phenomenon, the simulation using the 2D network sticks reproduces this hypothesis. In the series of voltage maps shown in Fig. 5d, we observe the origin of the crack formation as the tip of the vertical defect. This origin point for the crack propagation is the region where the electrical power is the highest, associated with higher local temperature, and therefore causing a local degradation of the nanowires in this area. This dynamic model mimics the hotspot creation and the associated defect propagation to the nearby region, and the Joule heating induced region turns it to a hotspot, which degrades drastically the next nearby nanowires. This catastrophic phenomenon propagates as a domino effect.

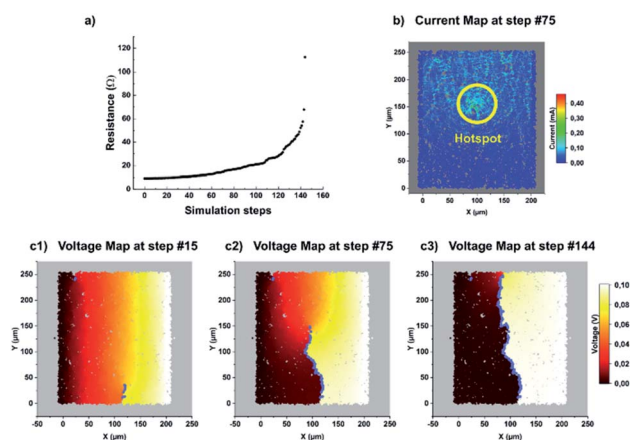


Fig. 4 Degradation of the simulated AgNW network. (a) Evolution of resistance of the simulated planar network until loss of percolation. Each step corresponds to a gradual increase of the macroscopic resistance, by removing a selected resistor. (b) Electrical current map at step 75. The bright region shows the highest current values, i.e. a hotspot. (c) Voltage maps are shown at different steps (15, 75 and 144). Blue dots mark the position of the successive removed resistors, representing the formation of the crack, and the loss of the percolation paths.

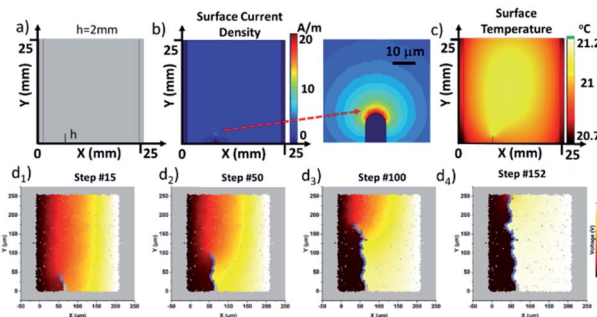


Fig. 5 Modelling the degradation in a AgNW network with an initial notch. (a) Scheme of a silver film with a 2 mm vertical notch at the bottom left of a $25 \times 25 \text{ mm}$ sample. (b) COMSOL simulation of the surface current density under a 1 V bias applied between the vertical opposite electrodes. Entire sample, and zoom on the notch area. (c) COMSOL steady-state simulation of the surface temperature distribution under a 1 V bias. (d) Voltage maps at different steps (15, 50, 100 and 152) representing the formation of the crack in a network with a vertical notch on a $200 \times 253 \mu\text{m}^2$ 2D stick simulated network obtained with the model proposed in the present article.



Conclusions and prospects

In this study we present a dynamic model capable of simulating the onset of the degradation of a metallic nanowire network subjected to electrical stress. The main electrical and thermal features of the simulated networks are compared with those of equivalent AgNW networks experimentally deposited. We used dynamic simulations based on the 2D stick percolation theory. Our model was designed to allow the modification of the percolation cluster, and it shows good agreement with respect to macroscopic resistance, electrical potential distribution and generated heat. A thorough comparison enables the deduction of an average junction resistance value of 14 Ω . The network degradation mostly originated from randomly localized exacerbated Joule-heating, which consequently leads to the local degradation of the AgNWs in that particular region of the sample. This localized damage propagates as a domino effect finally leaving behind a very thin, vertical region where the percolative nature of the network is lost. Such a region, following a strong analogy with a mechanical crack, destroys the electrical conduction paths. Our model also shows that regions with small defects can be the source of such hotspots, therefore inducing the electrical degradation of the whole specimen. The existence of a microscopic defect induces a large instability on the current density values along some tens of microns distance. Consequently, these simulations show also that the Joule heating in the edge of defects is much more significant than for the rest of the specimen, and thus it represents a plausible origin of a hotspot, as those experimentally observed. As a result, the present model provides deeper explanations related to the degradation mechanisms of metallic nanowire networks that have been experimentally observed, and thus paves the way for a better understanding of network failure. This is a necessary step to overcome instability issues in metallic nanowire based transparent electrodes in order to successfully integrate them into industrial devices.

Conflicts of interest

There are no conflicts to declare.

Acknowledgements

This work was performed within the framework of the Centre of Excellence of Multifunctional Architected Materials (CEMAM) no. ANR-10-LABX-44-01. Agence Nationale de la Recherche (ANR) is acknowledged for financial support under contracts ANR-18-CE09-0040 (MEANING) and ANR-18-CE09-0036 (PAN-ASSE). NC thanks Csaba Forró and Olivier Caudrelier for fruitful discussions.

References

- 1 D. S. Hecht, L. Hu and G. Irvin, *Adv. Mater.*, 2011, **23**, 1482–1513.
- 2 K. McLellan, Y. Yoon, S. N. Leung and S. H. Ko, *Adv. Mater. Technol.*, 2020, **5**, 1900939.
- 3 K. Ellmer, *Nat. Photonics*, 2012, **6**, 809–817.
- 4 D. Bellet, M. Lagrange, T. Sannicolo, S. Aghazadehchors, V. Nguyen, D. Langley, D. Muñoz-Rojas, C. Jiménez, Y. Bréchet and N. Nguyen, *Materials*, 2017, **10**, 570.
- 5 T. Sannicolo, M. Lagrange, A. Cabos, C. Celle, J.-P. Simonato and D. Bellet, *Small*, 2016, **12**, 6052–6075.
- 6 Y. Sun, M. Chang, L. Meng, X. Wan, H. Gao, Y. Zhang, K. Zhao, Z. Sun, C. Li, S. Liu, H. Wang, J. Liang and Y. Chen, *Nat. Electron.*, 2019, **2**, 513–520.
- 7 A. G. Ricciardulli, S. Yang, G.-J. A. H. Wetzelaer, X. Feng and P. W. M. Blom, *Adv. Funct. Mater.*, 2018, **28**, 1706010.
- 8 J. Wang, J. Jiu, T. Araki, M. Nogi, T. Sugahara, S. Nagao, H. Koga, P. He and K. Suganuma, *Nano-Micro Lett.*, 2014, **7**, 51–58.
- 9 D. T. Papanastasiou, A. Schultheiss, D. Muñoz-Rojas, C. Celle, A. Carella, J.-P. Simonato and D. Bellet, *Adv. Funct. Mater.*, 2020, 1910225.
- 10 H. H. Khaligh and I. A. Goldthorpe, *Nanoscale Res. Lett.*, 2013, **8**, 235.
- 11 D. Chen, F. Zhao, K. Tong, G. Saldanha, C. Liu and Q. Pei, *Adv. Electron. Mater.*, 2016, **2**, 1600167.
- 12 M. Lagrange, T. Sannicolo, D. Muñoz-Rojas, B. G. Lohan, A. Khan, M. Anikin, C. Jiménez, F. Bruckert, Y. Bréchet and D. Bellet, *Nanotechnology*, 2016, **28**, 055709.
- 13 D. P. Langley, M. Lagrange, G. Giusti, C. Jiménez, Y. Bréchet, N. D. Nguyen and D. Bellet, *Nanoscale*, 2014, **6**, 13535–13543.
- 14 T. Sannicolo, N. Charvin, L. Flandin, S. Kraus, D. T. Papanastasiou, C. Celle, J.-P. Simonato, D. Muñoz-Rojas, C. Jiménez and D. Bellet, *ACS Nano*, 2018, **12**, 4648–4659.
- 15 J. Lienig and M. Thiele, *Fundamentals of Electromigration-Aware Integrated Circuit Design*, Springer Publishing Company, Incorporated, 1st edn, 2018.
- 16 T.-B. Song, Y. Chen, C.-H. Chung, Y. M. Yang, B. Bob, H.-S. Duan, G. Li, K.-N. Tu, Y. Huang and Y. Yang, *ACS Nano*, 2014, **8**, 2804–2811.
- 17 F. N. Kholid, H. Huang, Y. Zhang and H. J. Fan, *Nanotechnology*, 2015, **27**, 025703.
- 18 R. Benda, B. Lebental and E. Cancès, *J. Appl. Phys.*, 2019, **126**, 044306.
- 19 D. Langley, G. Giusti, M. Lagrange, R. Collins, C. Jiménez, Y. Bréchet and D. Bellet, *Sol. Energy Mater. Sol. Cells*, 2014, **125**, 318–324.
- 20 D. P. Langley, M. Lagrange, N. D. Nguyen and D. Bellet, *Nanoscale Horiz.*, 2018, **3**, 545–550.
- 21 R. M. Mutiso and K. I. Winey, *Phys. Rev. E*, 2013, **88**, 032134.
- 22 S. De, T. M. Higgins, P. E. Lyons, E. M. Doherty, P. N. Nirmalraj, W. J. Blau, J. J. Boland and J. N. Coleman, *ACS Nano*, 2009, **3**, 1767–1774.
- 23 C. Forró, L. Demkó, S. Weydert, J. Vörös and K. Tybrandt, *ACS Nano*, 2018, **12**, 11080–11087.
- 24 R. M. Mutiso, M. C. Sherrott, A. R. Rathmell, B. J. Wiley and K. I. Winey, *ACS Nano*, 2013, **7**, 7654–7663.
- 25 C. Mayousse, C. Celle, E. Moreau, J.-F. Mainguet, A. Carella and J.-P. Simonato, *Nanotechnology*, 2013, **24**, 215501.



- 26 C. G. da Rocha, H. G. Manning, C. O'Callaghan, C. Ritter, A. T. Bellew, J. J. Boland and M. S. Ferreira, *Nanoscale*, 2015, **7**, 13011–13016.
- 27 A. A. Hagberg, D. A. Schult and P. J. Swart, *Proceedings of the 7th Python in Science Conference*, Pasadena, CA USA, 2008, pp. 11–15.
- 28 A. Bid, A. Bora and A. K. Raychaudhuri, *Phys. Rev. B: Condens. Matter Mater. Phys.*, 2006, **74**, 035426.
- 29 J.-Y. Lee, S. T. Connor, Y. Cui and P. Peumans, *Nano Lett.*, 2008, **8**, 689–692.
- 30 F. Selzer, C. Floresca, D. Knepe, L. Bormann, C. Sachse, N. Weiß, A. Eychmüller, A. Amassian, L. Müller-Meskamp and K. Leo, *Appl. Phys. Lett.*, 2016, **108**, 163302.
- 31 A. T. Bellew, H. G. Manning, C. G. da Rocha, M. S. Ferreira and J. J. Boland, *ACS Nano*, 2015, **9**, 11422–11429.
- 32 F. Völklein, H. Reith, T. W. Cornelius, M. Rauber and R. Neumann, *Nanotechnology*, 2009, **20**, 325706.

